

# Effect of Diffusive and Convective Substrate Transport on Biofilm Structure Formation: A Two-Dimensional Modeling Study

Cristian Picioreanu,<sup>1,2</sup> Mark C. M. van Loosdrecht,<sup>1</sup> Joseph J. Heijnen<sup>1</sup>

<sup>1</sup>*Department of Biochemical Engineering, Delft University of Technology, Julianalaan 67, 2628 BC Delft, The Netherlands, telephone:*

*+31 15 2781551; fax: +31 15 2782355; e-mail: C.Picioreanu@tnw.tudelft.nl*

<sup>2</sup>*Department of Chemical Engineering, University Politehnica of Bucharest, Splaiul Independentei 313, 77206 Bucharest, Romania*

*Received 13 October 1999; accepted 30 March 2000*

**Abstract:** A two-dimensional model for quantitative evaluation of the effect of convective and diffusive substrate transport on biofilm heterogeneity was developed. The model includes flow computation around the irregular biofilm surface, substrate mass transfer by convection and diffusion, biomass growth, and biomass spreading. It was found that in the absence of detachment, biofilm heterogeneity is mainly determined by internal mass transfer rate of substrates and by the initial percentage of carrier-surface colonization. Model predictions show that biofilm structures with highly irregular surface develop in the mass transfer-limited regime. As the nutrient availability increases, there is a gradual shift toward compact and smooth biofilms. A smaller fraction of colonized carrier surface leads to a patchy biofilm. Biofilm surface irregularity and deep vertical channels are, in this case, caused by the inability of the colonies to spread over the whole substratum surface. The maximum substrate flux to the biofilm was greatly influenced by both internal and external mass transfer rates, but not affected by the inoculation density. In general, results of the present model were similar to those obtained by a simple diffusion-reaction-growth model. © 2000 John Wiley & Sons, Inc. *Bio-technol Bioeng* 69: 504–515, 2000.

**Keywords:** biofilm; mathematical model; two-dimensional; flow; convection; diffusion; reaction; growth; roughness; irregular geometry; lattice Boltzmann

## INTRODUCTION

Experimental research has shown that biofilms develop in a multitude of patterns (Gjaltema et al., 1994; Kugaprasatham et al., 1992). Traditionally, development of biofilms was seen as the formation of a layered structure growing from the substratum up. The use of one-dimensional biofilm models (for example, Rittmann and Manem, 1992; Wanner and Gujer, 1986) strengthened this view. All the property gradients (like those of substrate concentration, biomass

density, porosity, etc.) in these models are one-dimensional, varying only in the direction from the bulk liquid to the carrier surface. There is, however, significant spatial variability in biofilm density, porosity, surface shape, microbial activity, and distribution in clusters (de Beer et al., 1994; de Beer and Stoodley, 1995; Gjaltema et al., 1994). Bishop and Rittmann (1996) suggest that while one-dimensional models can be adequate for description alone, multidimensional modeling may be required for prediction of biofilm heterogeneity. In a model that predicts biofilm structural properties as surface shape, porosity, pore and channel sizes, these same properties are not only the output of the model but they determine also, as time elapses, the place where boundary conditions are applied.

Modeling the structural development of a biofilm is a challenge because of the complex interaction between many processes. The biofilm development is determined by “positive” processes, like cell attachment, cell division, and polymer production, which lead to biofilm-volume expansion, and “negative” processes, like cell detachment and cell death, which contribute to biofilm shrinking. By changing the balance between these opposing processes, biofilms with different structural properties like porosity, compactness, or surface roughness can be formed, as it was hypothesized by van Loosdrecht et al. (1995) and experimentally shown by Kugaprasatham et al. (1992) and Kwok et al. (1998).

Biofilm expansion is mainly due to bacterial growth and production of extracellular polymers. Nutrients necessary for bacterial growth are dissolved in the liquid flow and reach the cells by passing first through the mass transfer-boundary layer (external mass transfer) and then through the biofilm matrix (internal mass transfer). The external mass transfer resistance is given by the thickness of the concentration boundary layer (CBL), which is directly correlated to the hydrodynamic boundary layer (HBL) resulting from the flow pattern over the biofilm surface. On one hand, the fluid flow drives the biofilm growth by regulating the concentra-

*Correspondence to:* C. Picioreanu

Contract grant sponsor: the Netherlands Organisation for Applied Scientific Research

Contract grant number: 95/638/MEP

tion of substrates and products at the liquid–solid interface. On the other hand, the flow shears the biofilm surface, eroding the biofilm structural protuberances. While the flow changes the biofilm surface, the interaction is reciprocal because a new biofilm shape leads to a different place of boundary condition, thus different flow and concentration fields. This further leads to the concept of temporal heterogeneity: The biofilm is a dynamic structure evolving in non-steady-state conditions.

For a biofilm model capable of full description of the three-dimensional heterogeneity, it is of importance that the model can easily cope with a large variation in time constants and with a continuously changing liquid–biofilm irregular boundary. With this in mind, we started to develop a quantitative model based on a discrete algorithm (a cellular automaton approach; Picioreanu, 1996). Similar approaches have been independently reported by Wimpenny and Colasanti (1997) and Hermanowicz (1998, 1999). Although these later models generate biofilms with qualitative features somehow resembling observed biofilms, these models work in a completely abstract time and space. There is no direct link between model parameters and real values of some widely accepted parameters as diffusivities, reaction rate constants, etc. Moreover, we found that for some of the processes a traditional differential approach is not only computationally but also conceptually more advantageous, which led to a combined discrete-differential model for the formation of biofilms (Picioreanu et al., 1998a,b). This model described in a quantitative way formation of 2-D and 3-D biofilm spatial heterogeneity due to diffusion–reaction–growth processes, by a combination of differential equations and cellular automata approaches. However, biofilm development was simulated in the absence of convective-mass flux.

Besides diffusion, convection is important for the overall mass transport toward the biofilm. Experiments by de Beer and Stoodley (1995) have shown that the concentration boundary layer can be parallel to the substratum (at low-flow velocity) but can also follow the biofilm shape (at higher flow velocity). The first case is analogous to our previous model of biofilm formation (Picioreanu et al., 1998b). However, to model the later case requires calculation of the flow pattern around the biofilm surface. Modeling fluid flow will also eventually give the possibility of modeling detachment due to liquid shear stress (Picioreanu et al., 1999). Recently, we (Picioreanu et al., 2000) described the influence of convective transport on substrate conversion in geometrically heterogeneous biofilm structures. A first effort to explain biofilm heterogeneity with a 2-D model including hydrodynamic processes, substrate transport by diffusion and convection, biomass growth and spreading is reported in Picioreanu et al. (1999). The present study provides a detailed description of the model. The model is used to systematically investigate the role of fluid flow, internal and external nutrient mass transport and inoculum distribution on development of the biofilm structure.

## MODEL FORMULATION

### Physical Description

The final goal is to build a model that can generate a *quantitative* description of the relationship between biofilm geometrical heterogeneity and different environmental conditions. In Picioreanu et al. (1998b) substrate diffusion, conversion and biomass growth were considered and the model presented there already produced a large range of biofilm morphologies. The biofilm formation was studied there only in hydrostatic conditions, where diffusion is the only mass transport mechanism. However, it is recognized that the hydrodynamic conditions have a decisive influence on the biofilm development (Characklis et al., 1982; Kugaprasatham et al., 1992; Picologlou et al., 1980). The model described in this article therefore includes: (1) liquid flow around the biofilm, (2) substrate mass transport by diffusion and convection in the liquid phase and by diffusion only in the biofilm-gel matrix (3) substrate conversion and biomass growth, and (4) biomass spreading based on cellular automata.

Biofilm detachment due to liquid-shear stress or due to sloughing represents another influence on biofilm structure, which is counteracting growth. In this stage of biofilm modeling this process is however neglected, because of lack of enough quantitative knowledge of mechanical properties and of local detachment mechanisms in biofilms. The biofilm is considered a rigid structure. Therefore, vibration of filaments, causing perturbations of the liquid-flow pattern and possibly increased mass transfer, is not taken into account.

There is a multitude of interesting biofilm systems within flowing system that can be modeled. Some of these systems are considered more representative, while others only scarcely occur in nature. Nevertheless, regarding hydrodynamics, three important aspects must be defined from the beginning: the geometry of the model system, the geometry of the substratum, and how the fluid flow is generated. In this study, we focused on one of the simplest cases: biofilm development on planar surfaces. The physical system is analogous with a standard parallel-plate flow cell (e.g., De Beer et al., 1994). The liquid medium, carrying nutrients, flows in laminar conditions through a narrow duct between two parallel plates. The flow is generated by pressure gradients. Without biofilm deposited on the plates, a fully developed Poiseuille (pressure-driven) flow would lead to purely axial velocity (in  $x$  direction), with variation only in the lateral coordinates ( $y$  direction). Thus, a fully-developed parabolic-velocity profile defines the inlet boundary condition. At the outlet, constant pressure and zero-gradient of velocity in axial direction are set. It is reasonable to assume an axi-symmetric system geometry, with equal biofilm formation on both top and bottom plates. This means that only half of the flow duct needs to be modeled, which obviously saves computational time and memory requirement. Consequently, a symmetry condition at the top boundary was set

both for flow variables and for substrate concentration. The bottom plate and the biofilm surface are considered no-slip walls. The two-dimensional reduction of the modeled system assumes that no gradients of any kind occur in the third ( $z$ ) direction. This means that both the plates and the biofilm grown on them extend infinitely in  $z$ -direction. The parabolic-velocity profile imposed in inlet was kept constant in time. This is equivalent to sending a constant liquid-flow rate through the channel. Due to biofilm growth, the hydraulic cross-section will decrease in time. Consequently, the mean fluid velocity in the region covered with biofilms will increase with an increasing biofilm thickness.

## Mathematical Description

The computational domain  $\Omega$  is discretized into a uniform grid of rectangular computational cells (Fig. 1). A grid cell is either occupied by solids (i.e., contains biomass or carrier in the subdomain  $\Omega_2$ ) or by liquid (i.e., in the subdomain  $\Omega_1$ ) as it was proposed in Picioreanu et al. (1998a) and Eberl et al. (1999). Biomass density in each grid element,  $c_X(t,x,y)$ , follows from a biomass growth equation:

$$\frac{dc_X}{dt} = r_X(c_S, c_X) \quad (1)$$

where  $r_X$  is the growth rate ( $\text{kg m}^{-3}\text{s}^{-1}$ ) and  $c_S$  is the local substrate concentration ( $\text{kg m}^{-3}$ ). By assuming only one limiting substrate (oxygen in our case), the rates of biomass formation,  $r_X$ , and of substrate consumption in the biofilm,  $r_S$ , were calculated in the present study according to the kinetic model suggested by Beffink et al. (1990):

$$r_X = Y_{XS}(r_S - m_S c_X) \quad (2)$$

$$r_S = \left( \frac{\mu_m}{Y_{XS}} + m_S \right) c_X \frac{c_S}{K_S + c_S} \quad (3)$$

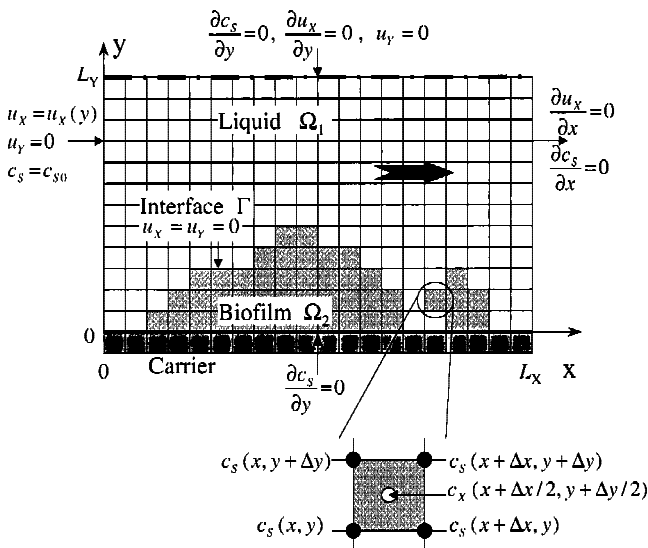


Figure 1. Model system definition.

where  $\mu_m$  is the maximum biomass growth rate ( $\text{s}^{-1}$ ),  $Y_{XS}$  is the yield of biomass on oxygen ( $\text{kg biomass kg}^{-1}$  substrate),  $m_S$  a maintenance coefficient ( $\text{s}^{-1}$ ) and  $K_S$  is the saturation constant for substrate ( $\text{kg m}^{-3}$ ). The same kinetic model was used also in Picioreanu et al. (1998a, 1998b).

When the biomass density in a grid cell reaches a certain maximum value,  $c_{Xm}$ , it will be partly redistributed to a neighbor cell, according to a set of local rules. In the following, we will call this discrete process the *biomass spreading step*, which uses a cellular automata description. Because little is known about preferential directions of bacterial division (hypothetically driven, for instance, by concentration or by pressure gradients), we preferred to keep these rules as simple as possible. An appropriate set of discrete rules, in which the newly formed biomass is redistributed in the neighboring space with no preferential direction, has been used in this work as formulated in Picioreanu et al. (1998a).

The substrate distribution in space,  $c_S(x,y)$ , necessary in the calculation of biomass growth rate, must be calculated from a mass-balance equation, set up in the whole computational domain. In steady state, the *convection-diffusion-reaction mass balance* is:

$$\mathbf{u} \cdot \nabla c_S = D_S \nabla^2 c_S + r_S(c_S, c_X) \quad (4)$$

where  $\mathbf{u}$  is the vector of liquid velocity ( $\text{m s}^{-1}$ ),  $D_S$  is the diffusion coefficient of substrate ( $\text{m}^2\text{s}^{-1}$ ),  $r_S$  is the rate of substrate consumption ( $\text{kg m}^{-3}\text{s}^{-1}$ ),  $c_S$  and  $c_X$  are the concentrations of substrate and biomass, respectively,  $\nabla$  is the divergence operator and  $\nabla^2$  is the Laplacian operator with respect to the spatial coordinates  $x$  and  $y$ . In the liquid compartment,  $\Omega_1$ , the reaction term is zero (no suspended biomass present). In the solid compartment,  $\Omega_2$ , the convective term vanishes (zero liquid velocity). Boundary conditions associated with equation (4) are:

$$c_S(0,y) = c_{S0} \quad \text{in inlet, at } y \in [0, L_Y] \quad (4a)$$

$$\frac{\partial c_S}{\partial x}(L_X, y) = 0 \quad \text{in outlet, at } y \in [0, L_Y] \quad (4b)$$

$$\frac{\partial c_S}{\partial y}(x, y) = 0 \quad \text{on the top and bottom boundaries, at } x \in [0, L_X], y = 0, y = L_Y \quad (4c)$$

The steady-state field of velocity,  $\mathbf{u} = (u_X, u_Y)$ , used to support the convective transport of substrate is given by the incompressible Navier-Stokes equations in laminar regime:

$$\mathbf{u} \cdot \nabla \mathbf{u} = -\frac{1}{\rho} \nabla p + \nu \nabla^2 \mathbf{u} \quad \text{and} \quad \nabla \cdot \mathbf{u} = 0 \quad (5)$$

where  $\mathbf{u}$  is the vector of liquid velocity,  $p$  is the pressure,  $\rho$  is the liquid density and  $\nu$  is the liquid kinematic viscosity. Two-dimensional Navier-Stokes equations are solved in the domain  $\Omega_1$  with boundary conditions:

$$u_x = u_y = 0 \quad \text{on biofilm-liquid interface} \quad (5a)$$

$$u_x(0,y) = u_{x,\max} \cdot (2y/L_Y - y^2/L_Y^2); u_y(0,y) = 0 \quad \text{in inlet, at } y \in [0, L_Y] \quad (5b)$$

$$\frac{\partial u_x}{\partial x}(L_X,y) = 0; u_y(L_X,y) = 0 \quad \text{in outlet, at } y \in [0, L_Y] \quad (5c)$$

$$\frac{\partial u_x}{\partial y}(x,L_Y) = 0; u_y(x,L_Y) = 0 \quad \text{on the top boundary, at } x \in [0, L_X] \quad (5d)$$

Solution of equations (5) will be referred later as the *hydrodynamic step*.

## Model Solution

### Time Scales

Processes in biofilms occur at very different time scales. One major problem we encountered was how to accommodate in the same biofilm model all the fast and slow physical, chemical, and biological processes. The solution comes from a time-scale analysis. The order of magnitude of the characteristic times for convective and molecular transport, biomass growth, biomass decay and detachment can be easily calculated by writing the model Equations (1)–(5) in a nondimensional form. By assuming, for example, a biofilm characteristic length of  $L = 0.5$  mm, diffusion coefficients in the range  $D_S = 5 \cdot 10^{-9} - 10^{-10} \text{ m}^2 \cdot \text{s}^{-1}$ , liquid kinematic viscosity  $\nu = 10^{-6} - 10^{-7} \text{ m}^2 \cdot \text{s}^{-1}$ , dissolved oxygen concentration  $c_S = 0.1-10 \text{ g} \cdot \text{m}^{-3}$ , biomass concentration in the biofilm  $c_X = 10-100 \text{ kg} \cdot \text{m}^{-3}$ , oxygen specific consumption rate  $q_S = 0.1-1 \text{ kg}_S \cdot \text{kg}_X^{-1} \cdot \text{h}^{-1}$ , biomass specific growth rate of  $\mu = 0.01-0.2 \text{ h}^{-1}$ , biomass specific decay rate  $k_d = 0.1-1 \text{ day}^{-1}$ , detachment rate  $k_{det} = 0.001-0.1 \text{ h}^{-1}$  and a fluid mean velocity  $u_x = 0.001-0.1 \text{ m} \cdot \text{s}^{-1}$ , the resulting characteristic times are shown in Figure 2.

It can be seen from Figure 2 that processes that change

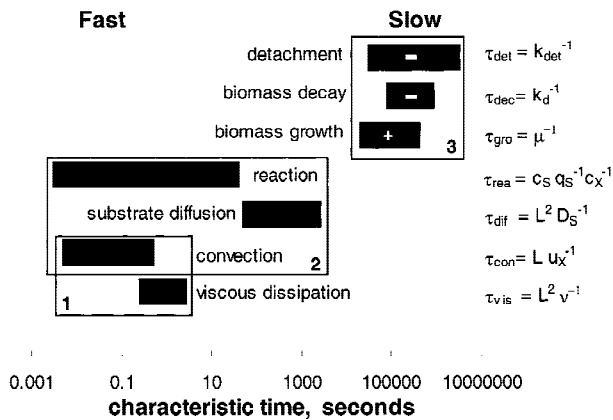


**Figure 2.** Characteristic times for some processes occurring in biofilms. (1) Processes in momentum balance, (2) processes in substrate mass balance, (3) processes in the biomass balance. In the present model only growth and decay of biomass are considered.

the biofilm volume (biomass growth, decay, and detachment) are all much slower than processes involved in substrate-mass balance (diffusion, convection, and reaction). Also, momentum transport (by convection or viscous dissipation) is much faster than the slowest step (i.e., diffusion) of substrate transfer. Usually, we are interested in the biofilm evolution during a few weeks of reactor operation. If the dynamic (nonsteady-state) balance equations for momentum, mass, and biomass growth were all solved with the smallest time-step, given in this case by the momentum equations, the computational effort needed to obtain the solution of substrate and biomass balances would be far too large. To achieve a realistic calculation speed, the natural time-scale separation in biofilm systems is very useful. Hence, we work at three time scales: (1) growth, in the order of hours or days, (2) mass transport of solutes, in the order of minutes, and (3) hydrodynamic processes, in the order of seconds. In other words, while solving the mass-balance equation, the flow pattern can be considered at pseudo-equilibrium for a given biofilm shape, and at the same time the biomass growth, decay, and detachment are in frozen state.

### Algorithm

The above considerations lead to the next strategy in following the biofilm development in time (Fig. 3):

1. A *hydrodynamic step* is performed each time the biofilm-liquid interface is modified. Momentum transfer and continuity Equations (5) are solved to find the flow-field variables: pressure  $p$ , velocities  $\mathbf{u}$ , and the normal and tangential stresses  $\tau$  acting on the biofilm surface. This step is needed each time when the geometry of the system has changed, for instance by growth (a positive development) or detachment (negative development).
2. The calculated flow velocities,  $\mathbf{u}$ , are used in solving the *convective-diffusive mass transfer* of soluble components (substrates, products), including also the *transformation processes* [Eq. (4)]. The mass-balance equation is solved toward a pseudo-steady state concentration of substrate,  $c_S$ . The substrate concentration at its turn will be used in the biomass growth kinetic equation. Both the Navier-Stokes equations and mass balance of substrate were solved in a dimensionless form by using a lattice Boltzmann algorithm (Chen et al., 1995; Chen et al., 1997; Picioreanu, 2000; Ponce Dawson et al., 1993).
3. The *new biomass content* of each grid element,  $c_X$ , is calculated by using Equation (2) including the substrate concentration at steady state calculated before. Typical time steps used in solving the growth process were between  $\Delta t_g = 1,000$  s for fast-growing biofilms to 10,000 s for slow-growing biofilms.
4. As biomass is growing, it has to be redistributed in space according to discrete (cellular automata) rules as used before in Picioreanu et al. (1998a, 1998b). The biomass content in the grid element in which it has grown above

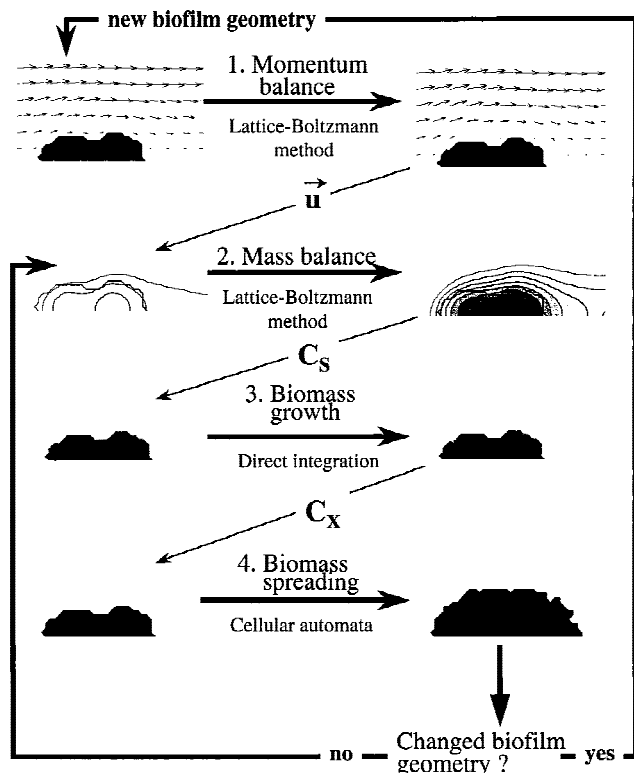


**Figure 3.** The general algorithm used to combine hydrodynamics, mass transport, biomass growth, and biomass spreading processes. The initial state of field variables characteristic of a process (symbolized by the pictures in the left side) is relaxed iteratively to a pseudo-steady state (pictures at the right side). Then, the next slower process takes place. When the biofilm geometry has changed, the whole cycle is repeated.

the maximum biomass density,  $c_{xm}$ , is split into two equal parts. Then, empty grid elements are occupied by pushing the neighbors to reach the free space. *Biomass spreading* generates the biofilm structure. On the other hand, this structure determines the further development of the biofilm by changing the flow behavior and the nutrients/products transport. After the biofilm volume expanded, the flow boundaries change and a new hydrodynamic step (step 1) is necessary. If biomass density did not exceed  $c_{xm}$  in any grid element, the mass balance (step 2) is solved using the same flow field.

By exploiting the natural time-scale separation in biofilms, the step by which the whole algorithm advances in time is the one necessary for the slowest process, namely growth,  $\Delta t_g$ . The loop through steps 1–4 is repeated a few hundred times to simulate the biofilm life of a few weeks. The whole process is at the moment computationally expensive because each time when the loop is executed both the flow and the concentration fields must be close to the steady state. Typically, the lattice Boltzmann algorithm we use to relax the flow field requires for a stable operation time steps,  $\Delta t_f$ , in the order of  $10^{-5}$ – $10^{-6}$  s, while for mass transfer  $\Delta t_m = 10^{-3}$ – $10^{-4}$  s is adopted. Tens of thousands relaxation steps are therefore required. Using as start values in each relax-

ation step the values from the previous steady state, the flow field usually relaxed in less than 0.01 s, while the concentration field approaches the new steady state in less than 5 s. Practically, the time-scale separation of flow, mass transfer, and growth processes is complete. The algorithm performance is a trade-off between imposed accuracy and speed. Speed can be considerably increased by: (1) increasing the time-step for growth if the biomass is less active, (2) incomplete relaxation of mass and momentum transfer equations, (3) performing the flow calculations only when the biofilm surface geometry has significantly changed, (4) using other numerical algorithms more efficient than lattice Boltzmann, and (5) parallelization of the computer code. The actual version of the model code was run on 8 or on 16 processors from a Cray T3E parallel machine with 128 processors at 400 MHz, at TU Delft. Typical runs take about one day of computations.

### Model Parameters

The distance between the parallel plates was 1 mm, hence, the height of the computational domain was  $L_y = 500 \mu\text{m}$ , with a length  $L_x = 2000 \mu\text{m}$ . Biomass inoculum was randomly distributed only between  $x = 400$  and  $x = 1600 \mu\text{m}$  to allow biomass spreading without exceeding the boundaries. Most of the biofilm kinetic parameters used (Table I), were taken from Picioreanu et al. (1998b); they correspond to growth of nitrifying biofilms. The growth-limiting substrate is dissolved oxygen.

Three factors that might influence the geometrical heterogeneity of biofilms were investigated: (1) internal substrate-transport limitation, (2) external resistance to mass transfer, and (3) the fraction of carrier surface initially covered with biomass. The ratio (maximum biomass growth rate)/(maximum internal transport rate of substrate), was proposed in Picioreanu et al. (1998b) as a factor determining the biofilm heterogeneity. The growth ratio,  $G$ , is calculated as  $G = (L_y^2 \mu_m c_{xm}) / (D_s c_{s0})$ . By setting the inlet dissolved oxygen concentration to  $c_{s0} = 0.4, 4, 8,$  and  $20 \text{ mg/L}$ ,  $G$  is taken as 562, 56, 28, and 11.

The intensity of substrate transport from the bulk liquid to the biofilm surface is characterized by mass transfer coefficients. Together with the surface shape, the flow regime determines the thickness of the boundary layer in which the external resistance to mass transport is mostly concentrated. The maximum inlet velocity,  $u_{x,max}$ , was 1 and 0.125 cm/s, which gives mean flow velocities in the channel,  $u_0 = 0.67$  and 0.08 cm/s, respectively. The corresponding Reynolds numbers,  $Re$ , based on the empty channel width and mean velocity were 6.7 and 0.8, respectively. The flow rate at which the liquid is driven through the channel is constant in time, unless otherwise specified.

Simulations at different  $Re$  and  $c_{s0}$  were performed starting with the same inoculum distribution on the bottom plate. However, the number of grid elements initially inoculated with biomass,  $n_0$ , was also varied where  $n_0 = 15, 30, 60,$  and 120. This inoculation corresponds to an initial surface-

**Table I.** Model parameters.

Model parameter	Symbol	Parameter value	Units
Physical system dimensions	$L_X \times L_Y$	2000 × 500	μm
Computational-grid dimensions	$N_X \times N_Y$	512 × 129	grid nodes
Bulk oxygen concentration	$c_{S0}$	$0.4 \cdot 10^{-3}$ , $4 \cdot 10^{-3}$ , $8 \cdot 10^{-3}$ and $20 \cdot 10^{-3}$	$\text{kg}_S \text{m}^{-3}$
Oxygen saturation constant	$K_S$	$3.5 \cdot 10^{-4}$	$\text{kg}_S \text{m}^{-3}$
Oxygen diffusion coefficient	$D_S$	$2.3 \cdot 10^{-9}$	$\text{m}^2 \text{s}^{-1}$
Liquid kinematic viscosity	$\nu$	$10^{-6}$	$\text{m}^2 \text{s}^{-1}$
Liquid density	$\rho$	1000	$\text{kg m}^{-3}$
Maximum velocity in inlet flow	$u_{X,max}$	$10^{-2}$ and $1.25 \cdot 10^{-3}$	$\text{m s}^{-1}$
Number of grid elements inoculated with biomass	$n_0$	15, 30, 60 and 120	—
Maximum biofilm biomass density	$c_{Xm}$	30	$\text{kg}_X \text{m}^{-3}$
Biomass yield on substrate	$Y_{XS}$	0.045	$\text{kg}_X \text{kg}_S^{-1}$
Maintenance coefficient	$m_S$	$3 \cdot 10^{-5}$	$\text{kg}_S \text{kg}_X^{-1} \text{s}^{-1}$
Biomass maximum specific growth rate	$\mu_m$	$1.5 \cdot 10^{-5}$	$\text{s}^{-1}$

grid coverage,  $s_0$ , equal 5%, 10%, 20%, and 40%, respectively. Because in the mathematical model each inoculated grid volume gets a random initial concentration of biomass, between 0.2 and 0.9 from the maximum  $c_{Xm}$  allowed, the physical surface coverage is, in fact, significantly smaller than the values of  $s_0$  shown above.

### Biofilm Measures

To quantify the simulated biofilm structure, measures like biofilm area enlargement ( $\alpha$ ), coefficient of surface roughness ( $\sigma$ ), compactness ( $\xi$ ), porosity ( $\epsilon$ ) and maximum biofilm thickness ( $\delta$ ) were used as defined in Picioreanu et al. (1998b). An additional parameter presented, the surface-grid coverage  $s$ , is the fraction of carrier surface covered with grid cells containing biomass. The overall flux of oxygen per carrier area ( $\Phi_{S,C}$ ,  $\text{g O}_2 \text{m}^{-2} \text{carrier s}^{-1}$ ) was calculated by numerical integration of the substrate conversion rate in the biofilm volume:

$$\Phi_{S,C} \approx \frac{(\Delta x)^2}{L_X} \sum_{(x,y) \in V_b} r_S(c_S(x,y)) \quad (6)$$

where  $\Delta x$  is the grid-step size.

To avoid, as much as possible, perturbations in biofilm statistical measures due to the rapid growth rate near the entrance, all structural and functional biofilm measures were calculated only between  $x = 500$  and  $x = 1600$  μm.

## RESULTS AND DISCUSSION

### Biofilm Development in Time

The evolution of two simulated biofilms in time is presented in Figure 4a–d, for a transport-limited case (high metabolic rates,  $G = 562$ ,  $s_0 = 5\%$ , and  $Re = 6.7$ ), and in Figure 4e–h for a microbial growth-limited regime (low metabolic rates,  $G = 11$ ,  $s_0 = 5\%$ , and  $Re = 0.8$ ). At the beginning, when there is enough substrate in the environment (i.e., there is no important nutrient limitation), the biofilm grows

in hemispherical colonies. Due to the nutrient availability, biomass equally expands in all directions (Fig. 4a, 4e, and 4f). We could call this growth regime *isotropic biofilm expansion*.

As the film gets thicker, two situations can occur. If there is still no substrate limitation (i.e., low  $G$ ) or the colonies are close enough to each other (i.e., dense initial colonization, at high  $s_0$ ), then the separate clusters will merge into a continuous microbial film (Fig. 4g and 4h). Eventually, the whole carrier surface will be covered (Figs. 4h and 7a).

The other possible scenario is when the nutrient is depleted in the biofilm depth. In this case, there is almost no flux of substrate to the cells situated in the “valleys.” Because only microbes in the top regions are active, dividing and creating new biomass, biofilm growth becomes unidirectional. Colonies grow as “fingers” or “filaments” toward the liquid bulk. In general, for uniformly distributed biomass on the carrier the preferential growth direction is perpendicular to the carrier surface. Colonies without competitors in the neighborhood, however, can expand in any direction where substrate is available. This is valid especially for the colonies situated near to the substrate entrance (see Fig. 4d). Therefore, biofilm structural measures were calculated only from  $x = 500$  μm until  $x = 1600$  μm.

Figure 5 presents biofilm geometry together with the distribution of substrate concentration, resulting from twelve simulations at variable  $G$ ,  $Re$ , and  $s_0$ . The same as shown in Figure 4d, Figure 5a, 5d, 5g, and 5j show examples of branched colonies formed near the substrate inlet. Figures 6 and 7 show biofilm geometrical characteristics coefficient of roughness,  $\sigma$ , compactness,  $\xi$ , area enlargement,  $\alpha$ , surface-grid coverage,  $s$ , porosity,  $\epsilon$ , and the substrate flux per carrier area  $\Phi_{S,C}$ , as functions of achieved biofilm maximum thickness,  $\delta$ . The achieved biofilm thickness was chosen as abscissa instead of time, due to the very different time scales at which biofilms develop in different conditions. For instance, at  $G = 562$  and  $s_0 = 10\%$  the 150 μm thickness was reached in 88 days, while at  $G = 11$  and  $s_0 = 40\%$  the same thickness was obtained in only 4 days (see Fig. 6e).

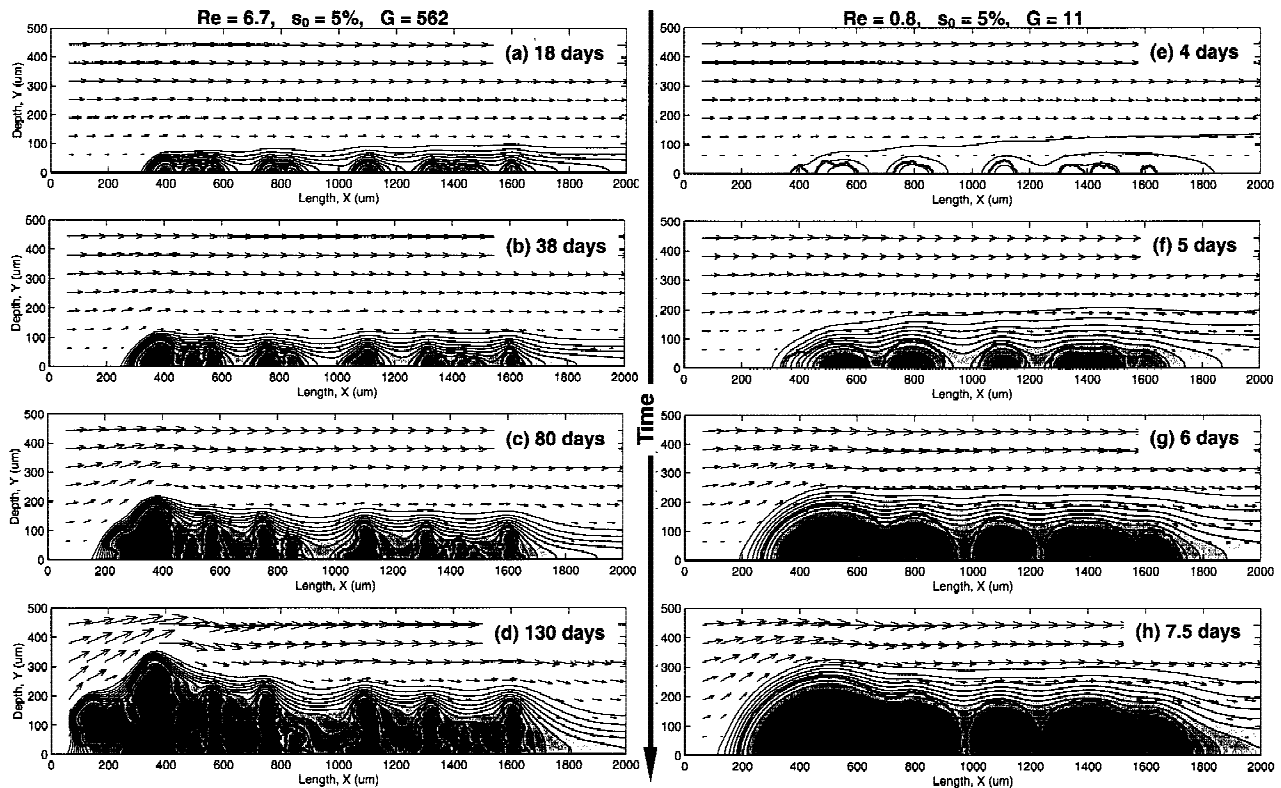


**Figure 4.** Simulated biofilm evolution in time for (a–d)  $Re = 6.7$ ,  $s_0 = 5\%$ ,  $G = 562$  and (e–h)  $Re = 0.8$ ,  $s_0 = 5\%$ ,  $G = 11$ . The arrows represent the vector velocity at intervals of 16 grid nodes. The thick lines indicate the biofilm surface. Iso-concentration lines show the decrease of substrate concentration from the maximum value in the bulk liquid (white patches) to zero in the biofilm (dark gray patches), with a variation of 10% between lines.

### Roughness

In the kinetic-limited regime ( $G = 11$ ), smooth biofilms are generally obtained. After the initial voids between colonies are filled with biomass, roughness gradually decreases, approaching almost asymptotically values less than  $\sigma < 0.1$  (Fig. 6a and 6d). At low velocity ( $u_{X,max} = 0.00125$  m/s,  $Re = 0.8$ ) and low inoculation however, insufficient substrate was supplied and the resulted structure showed deep pores. In the transport-limited regime ( $G = 562$ ), very rough biofilms formed, regardless of the inoculation density. Even for  $s_0 = 40\%$ , after covering all carrier surface (Fig. 7a), competition between colonies generated a strong irregularity of biofilm surface (Fig. 6d). At intermediate  $G = 56$ , the inoculation density played an important role. One might obtain either smooth (Figs. 6d and 5k) or rough (Figs. 6d and 5h) structures.

### Porosity

While roughness measures the biofilm surface deviation from a mean thickness, porosity indicates a volumetric irregularity of biofilm structure. Variation of porosity in time (Fig. 7b) is similar to that of roughness. Starting with values close to 1 (sparse distribution of inoculum cells) porosity initially decreases in the isotropic expansion period, to approach later a quasi-steady-state in the transport-limited period.

### Compactness

This measure is a special kind of *shape factor*, widely used in image analysis. Basically, it shows a trend that is opposite to biofilm porosity (Fig. 6b and 6e).

### Area Enlargement

It is a measure of biofilm-surface irregularity. After the isotropic growth period, area enlargement soon approaches a constant and small value ( $\alpha = 1-1.5$ ) in the growth-limited regime ( $G = 11$ ). At higher  $G$ , area enlargement  $\alpha$  will show an almost linear increase (Fig. 6c and 6f), corresponding to the appearance of filamentous structures. The linear increase of  $\alpha$  with the biofilm thickness is explained by the fact that “finger-like” colonies grow only in a vertical direction, forming only a new lateral area. It is important to mention that this lateral area *cannot* significantly participate to mass transfer (Picioreanu et al., 2000), unless, for example, filament oscillation enhances the turbulent transport of substrate to the biofilm surface. In fact, as theoretically demonstrated in Picioreanu et al. (2000), for rigid structures the external mass transfer even decreases with a higher  $\alpha$ .

### Substrate Flux Per Carrier Area

Two phases can be distinguished in the evolution of substrate flux (Fig. 7c and 7f). There is first a sharp increase, corre-

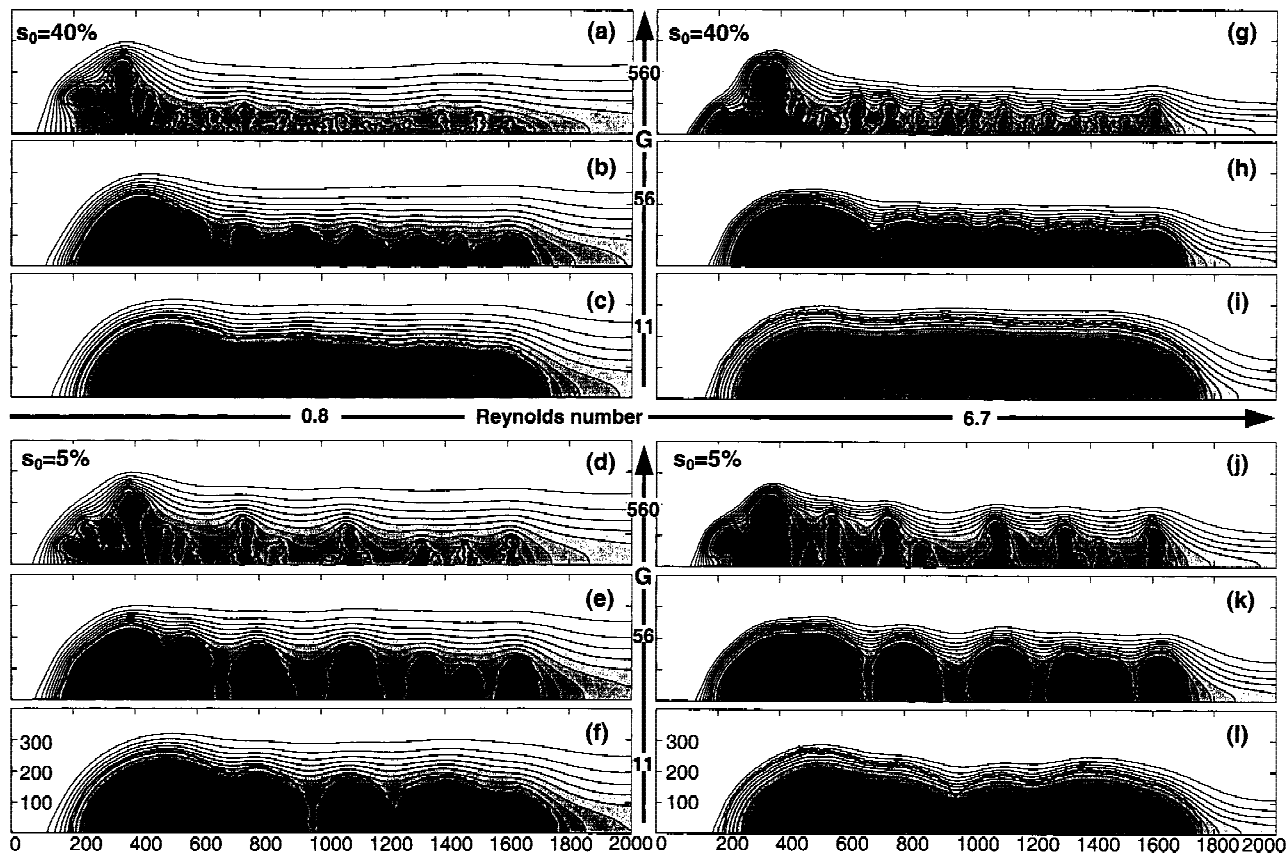


**Figure 5.** Influence of environmental conditions on biofilm development. Lines and gray shades have the same meaning as in Figure 4. All structures are shown at a maximum biofilm thickness of 250  $\mu\text{m}$ . The scale is in  $\mu\text{m}$ , the same for all graphs.

sponding to the isotropic growth. As the film thickness grows, the substrate will be able to penetrate only a superficial layer with a certain thickness. Only in that active layer can transformations occur, thus the substrate conversion becomes limited by internal mass transport. The consequence is a plateau in substrate flux. What is interesting is that also for the filamentous biofilms grown at  $G = 562$ , the substrate flux reaches a plateau. Combining this information with the growing evolution of the biofilm area in these conditions, we come once again (Picioreanu et al., 2000) to the conclusion that (at least) in rigid biofilms developed on planar surfaces, conversion does not enhance with an increase in surface area. The  $G$ -ratio seems to be the main determining factor for the achievable substrate flux. By using a simplified mass transport model, Rittmann et al. (1999) addressed this issue in the same way, coming to a similar conclusion: The average flux of nutrient per carrier area can be increased by the cluster-and-channel type of biofilm *only if* there is enough convection in the biofilm valleys.

### Effects of Mass Transport, Flow Velocity, and Inoculation Density

#### Internal Mass Transport— $G$ Ratio

As seen from the definition of  $G$  ratio, a high value of  $G$  means mass transfer limitation, while a lower one means a

limitation of biofilm development by microbial growth rate. Mass transfer limitation occurs in thick biofilms ( $L_Y \gg \lambda$ ), with very active or dense biomass ( $\mu_m c_{Xm} \gg \mu_m c_{S0}$ ), in systems with slow internal diffusion rates of limiting substrates ( $D_S \ll \lambda^2$ ) or at low nutrient concentration in the bulk ( $c_{S0} \ll c_{S0}^*$ ). Smoother ( $\sigma \rightarrow 0$ ,  $\alpha \rightarrow 1$ ) and more compact ( $\xi \rightarrow 1$ ) biofilms were always generated by the model at low  $G$  ratios, i.e., in a growth regime not limited by substrate mass transfer. Figure 8 clearly shows these trends of biofilm properties, measured when biofilm thickness (only between  $x = 500$  and  $x = 1600 \mu\text{m}$ ) reached 150  $\mu\text{m}$ .

The overall progress of biofilm roughness, compactness, area enlargement (Fig. 6) and porosity (Fig. 7) computed with this model, including convective transport of substrate, is very similar to that computed with the simplified diffusion-reaction-growth model (where convective transport is not taken into account; Picioreanu et al., 1998b).

#### Inoculation Density

Initial adhesion of microbes—or reattachment of detached cells—on the substratum surface could have major effects on the later biofilm development. As experimental studies have often demonstrated (Gjaltema et al., 1997; Verran et al., 1991), micro-roughness of carrier surface promotes initial microbial colonization. Physical properties (charge, hy-



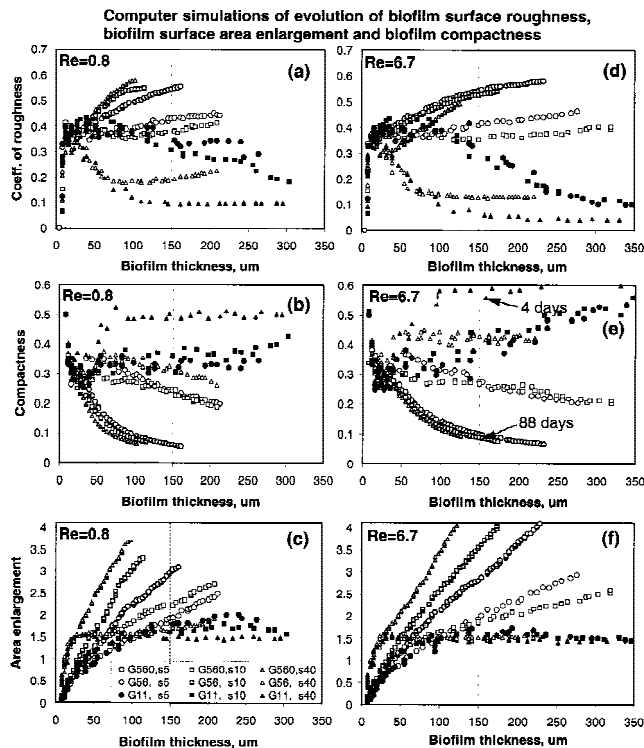


**Figure 6.** Variation of coefficient of surface roughness, biofilm compactness, and surface-area enlargement during growth, as a function of biofilm thickness, at (a–c)  $Re = 0.8$  and (d–f)  $Re = 6.7$ . Symbols are values at  $G = 560$  (gray), 56 (white), and 11 (black symbols);  $s_0 = 5\%$  (circles), 10% (squares), and 40% (triangles). All data points are computer-model results.

drophobicity) also affect microbial distribution on the carrier surface (van Loosdrecht et al., 1987). Starting the simulations with different initial fractions of covered substratum,  $s_0$ , can be interpreted as a simplistic way to include influences of the substratum properties on further biofilm growth.

In general, a smaller fraction of substratum surface colonized (i.e., less attachment) leads to a rougher biofilm. This can be clearly seen by comparing the structures from Figure 5e and 5k ( $s_0 = 5\%$ ) with those in Figure 5b and 5h ( $s_0 = 40\%$ ), respectively. Roughness is in this case caused by the inability of the colonies to cover the whole surface (Fig. 7a). Deep vertical voids result from nutrient depletion in the biofilm depth. Because the substrate comes from the bulk liquid, the colonies *naturally* tend to grow in the direction of the maximum substrate concentration (vertical direction here). This leaves large spaces between colonies, channels that cannot be filled by a lateral biofilm expansion. It is, therefore, not necessary to introduce a *preferential* mechanism of biofilm spreading (e.g., chemotactic) to find a rational explanation for biofilm vertical voids or pores. However, in reality detached cells can reattach on the available substratum. Even though later colonization of pores is possible, further growth and filling up is impeded by the very low nutrient availability.

More cells initially agglomerated on the same substratum area means more competition for resources. Thus, especially at low substrate concentration, all the cells suffer substrate limitation. This is why, at the highest initial surface

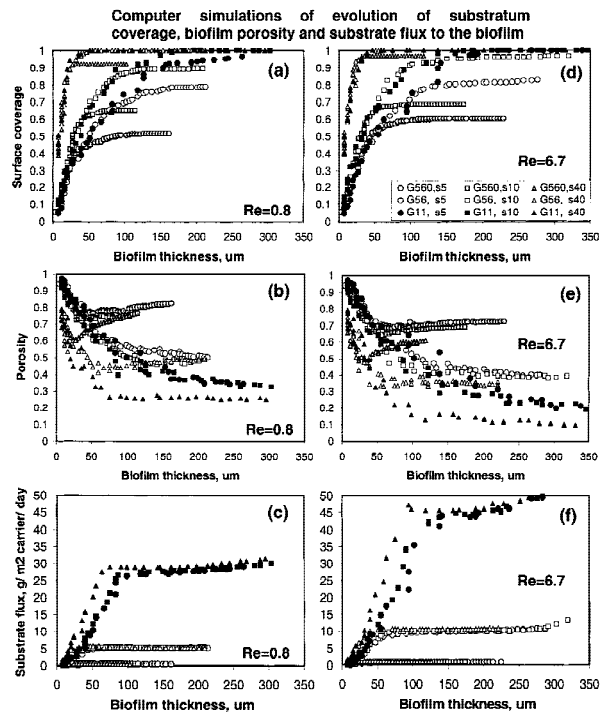


**Figure 7.** Variation of carrier-surface coverage, biofilm porosity, and substrate flux per carrier area during growth, as a function of biofilm thickness, at (a–c)  $Re = 0.8$  and (d–f)  $Re = 6.7$ . Signification of symbols is the same as in Figure 6. All data points are computer-model results.

colonization ( $s_0 = 40\%$ ), the biofilm roughness at  $\delta = 150 \mu\text{m}$  increased (Fig. 6a), compactness was lower (Fig. 6b) and the area enlargement was considerably greater (Fig. 6c) than at low  $s_0$ . After a few colonies succeed in dominating the others in the competition for substrate, the general aspect of biofilm growth is very similar to that at low-surface inoculation.

The combined influence of mass transfer and inoculation density on biofilm structure can be presented in diagrams like Figure 9. Contours of roughness coefficient were con-

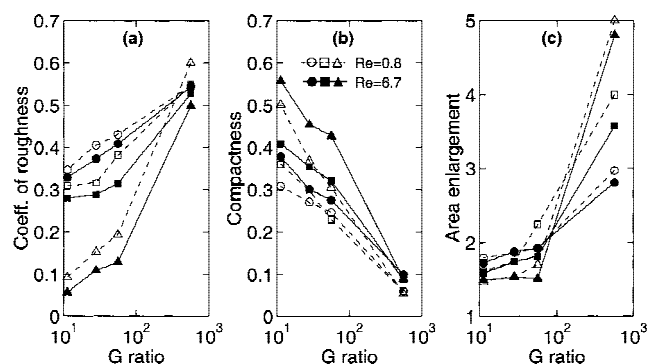


**Figure 8.** Variation of (a) coefficient of surface roughness, (b) biofilm compactness, and (c) surface-area enlargement, with the  $G$  ratio. These measures were taken at a biofilm maximum thickness of  $150 \mu\text{m}$  between  $x = 500$  and  $x = 1600 \mu\text{m}$ . Continuous lines show simulation results for the high-liquid velocity ( $0.01 \text{ m/s}$ ,  $Re = 6.7$ ), dashed lines for the low velocity ( $0.012 \text{ m/s}$ ,  $Re = 0.8$ ). The inoculation density was  $s_0 = 5\%$  (circles), 10% (squares), and 40% (triangles).

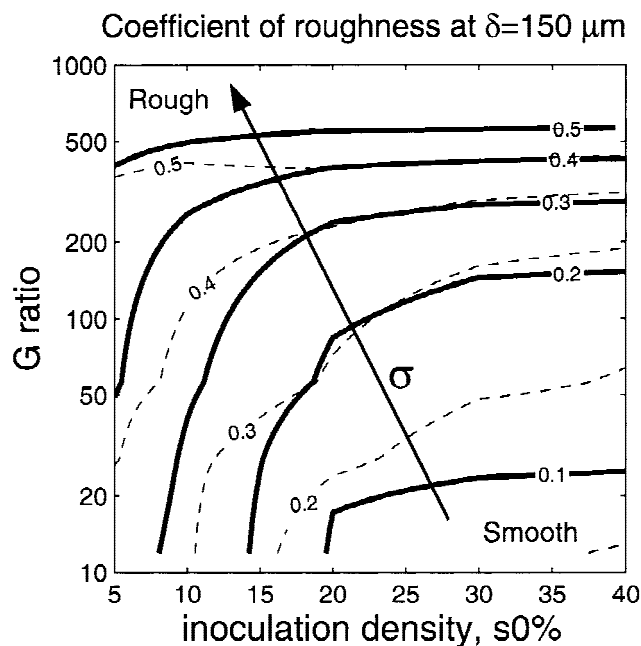


**Figure 9.** Dependence of biofilm coefficient of roughness on  $G$  ratio and on  $s_0$ . The coefficient of roughness was measured when the biofilm was  $150\ \mu\text{m}$  thick. Thick lines are iso-roughness contours at  $Re = 6.7$ , and thin lines are at  $Re = 0.8$ .

structured with results of simulations at  $G = 562, 56, 28,$  and  $11$  and  $s_0 = 5, 10, 20, 30,$  and  $40\%$ , at  $u_{X,max} = 0.01\ \text{m/s}$ . Completely smooth biofilms can be obtained only at low  $G$  and high-inoculation density. By crossing a transition zone, rough biofilms are obtained both at low initial adhesion ( $s_0 \ll$ ) and at substrate transport limitation ( $G \gg$ ).

### Flow Velocity

A higher flow velocity decreases the thickness of the hydrodynamic boundary layer and, consequently, the thickness of the concentration boundary layer (CBL). This can be clearly seen by comparing the CBL thickness at  $u_{X,max} = 0.0012\ \text{m/s}$  in Fig. 5a–f (approx.  $100\text{--}150\ \mu\text{m}$ ) with that at  $u_{X,max} = 0.01\ \text{m/s}$  in Fig. 5g–h (between  $25\text{--}100\ \mu\text{m}$ ). The resistance in the CBL diminishes, thus the mass-transfer coefficient increases leading to a higher flux of substrate to the biofilm. There are two consequences: (1) the biofilm grows faster; (2) more compact and smooth structures develop. The simulation results at an achieved maximum biofilm thickness of  $150\ \mu\text{m}$  clearly show that the coefficient of surface roughness (Fig. 8a), as well as the area enlargement (Fig. 8c), were always higher at low  $Re$  ( $Re = 0.8$ , dashed lines with open symbols) than at high  $Re$  ( $Re = 6.7$ , continuous lines with filled symbols). In the same conditions, a less compact biofilm results at the lower  $Re$  number than at the high one (Fig. 8b).

It is clear that a faster flow over the biofilm can increase the biofilm compactness because of a higher biomass formation rate. One must consider, on the other hand, that higher  $Re$  also means higher shear stress on the biofilm

surface. The detachment rate by continuous erosion of surface irregularities would increase, leading to a smooth but thinner biofilm. Moreover, having a jelly and flexible structure, the filaments grown at very high  $G$  and high liquid velocity (Fig. 5j) could vibrate and eventually break. Sloughing events are likely in such systems. The effect of the high  $Re$  regime on biofilm morphology found above should, therefore, not be considered isolated, as long as detachment resulted from shearing forces is not included in the model (van Loosdrecht et al., 1995, 1997).

From Figure 5 it can be appreciated that, in the range of velocities studied, the CBL was, in most of the cases, parallel to the substratum surface (unless in entrance or in case of individual colonies). With only small deviations, this was observed also at  $u_{X,max} = 1\ \text{cm/s}$  and at low-inoculum distribution on the support. These observations raise an important question: are flow-field computations really needed in a multidimensional model for biofilm structure, and if yes, when? In the planar case, the thickness of the CBL can be estimated from the mass transfer coefficient, which results from experimental or theoretical correlations. In this case, a simplified model including only diffusive transport of substrate through the CBL, as presented in Picioreanu et al. (1998b), could be satisfactory. This approach has an obvious advantage: It skips the computationally expensive flow calculations. However, flow pattern might be needed when: (1) the biofilm clusters are far away from each other and the liquid velocity in the bulk is so high that significant convective substrate transport is possible in the channels, (2) biofilm maximum thickness varies considerably along the carrier surface (as in Fig. 5d–f, for instance) and so does also the CBL thickness, (3) the wall-shear stress must be known to implement local biofilm detachment rules.

### Detachment Effects

The present model does not include biofilm detachment, which certainly determines biofilm structural characteristics (Kwok et al., 1998). The results detailed above can be influenced by detachment in many ways. Erosion, seen as the continuous removal of small particles from the biofilm–liquid interface, makes a smoother biofilm surface. Conversely, sloughing events (loss of big biofilm patches, usually broken near the biofilm–substratum interface) lead to an increased biofilm–surface roughness. Moreover, newly attached cells deep in biofilm channels might get a chance to grow if old neighboring colonies break off and are washed away. An extension of the present model with a biofilm detachment mechanism due to mechanical stress caused by liquid flow, will be described in a forthcoming article.

### Effect of Flow-Driving Mechanism

The results shown above were calculated at constant flow-rate through the channel. This means that pumping the liquid must overcome an increasing frictional resistance due to channel obstruction with biofilms. The pressure difference

needed to drive the flow is continuously increasing (Fig. 10a). Another common case is when the flow is driven by a constant body force or at constant  $\Delta p$  (as in the experimental work of Picologlou et al., 1980). The body force can be easily imagined when the flow is generated by gravitational or centrifugal forces. A gravitational flow in a channel inclined at different angles can provide a large range of fluid velocities. In this case, because the driving force is constant and the fractional resistance is steadily increasing, the flow velocity and volumetric rate decrease (Fig. 10b). The expected effect would be: (1) a decreased flux of substrate entering the system, which leads to a greater variation of biofilm thickness along the channel length, and (2) an increased external mass transfer resistance, which makes the overall growth process decrease in time. Both effects were evaluated in a simulation at  $c_{SO} = 4 \text{ mg/L}$ , 5% initial coverage and initial maximum velocity  $u_{X,max} = 0.01 \text{ m} \cdot \text{s}^{-1}$ . The inlet and outlet boundaries were, in this case, connected to form a periodic space. The corresponding acceleration

needed to produce an initial  $u_{X,max} = 0.01 \text{ m} \cdot \text{s}^{-1}$  was  $g_X = 0.08 \text{ m} \cdot \text{s}^{-2}$ . This  $g_X$  was kept constant during the whole simulation.

In the first 5 days there was an exponential development, the biofilm growing in a kinetic-limited regime. Later, due to only about  $50 \mu\text{m}$  oxygen penetration depth, the biofilm growth becomes limited by substrate transport. The substrate flux (calculated for the biofilm at  $x \in [500,1600] \mu\text{m}$ ) tends to reach a plateau, while the thickness increases linearly because growth occurs only in a superficial layer. The effect of external mass transfer resistance becomes evident only after 7 days. At constant flow rate, the flux of substrate increases slightly due to less external resistance. At constant body force, due to the decreasing flow rate, the mass flux decreases as a result of a smaller mass transfer coefficient. Although the mean flow velocity dropped in the first 2 weeks of biofilm growth below 25% from the initial velocity, the flux of oxygen per carrier area decreased to only 70% (Fig. 10a). The maximum biofilm thickness achieved between 500 and 1600  $\mu\text{m}$  evolved almost at the same values (Fig. 10b). Moreover, the whole structure ( $\sigma, \xi, \alpha$ ) of the biofilm grown at constant force was almost identical to that grown at constant flow rate. This shows that, at least until the biofilm reaches a thickness less than half of the channel width, the way the flow is driven is less important. While external resistance to mass transfer does contribute to the overall substrate conversion rate, the major controlling mechanism is internal mass transfer resistance.

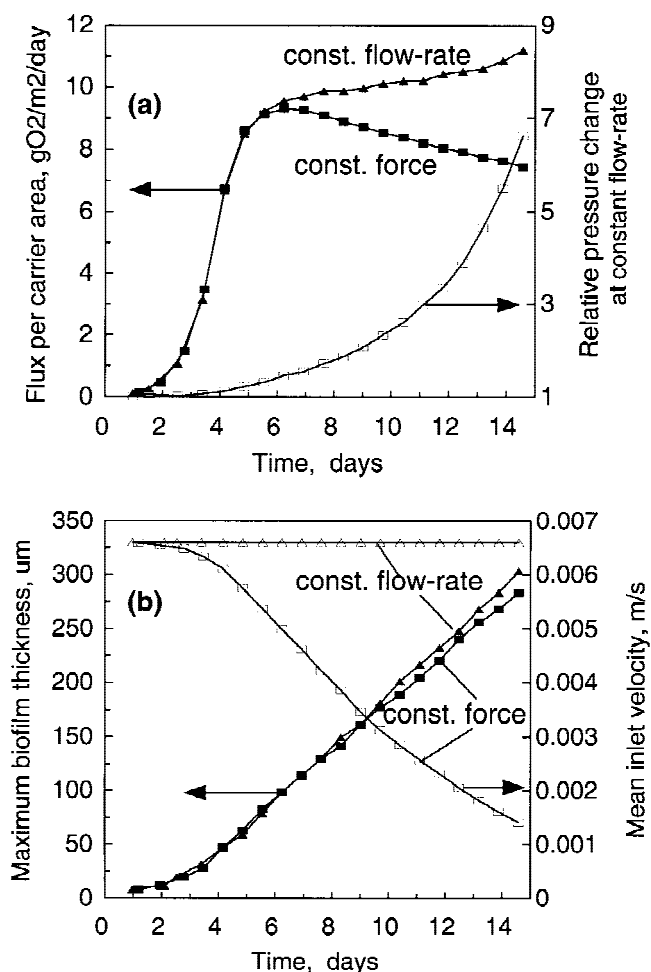


**Figure 10.** Comparison of biofilm characteristics evolving in time at constant flow rate and at constant driving force. (a) Substrate flux per carrier area and pressure change relative to the empty channel. (b) Maximum biofilm thickness on  $x \in [500,1000] \mu\text{m}$  and the average liquid velocity in the channel inlet.  $\Delta$  and  $\blacktriangle$ —constant liquid flow rate;  $\square$  and  $\blacksquare$ —constant driving force. All data points are computer-model results.

## CONCLUSIONS

1. A 2-D model was elaborated for biofilm development including biomass growth, diffusive and convective transport, and transformation of substrates and flow around the biofilm structure. The model is fully quantitative, being based on first principles as Navier-Stokes equations, substrates mass balances, and kinetic laws for biomass growth. Using a time-scale separation, processes with very different characteristic times are accommodated in a unitary model. Its computational effectiveness is a trade-off between the required accuracy and computational speed.
2. Using this model, three possible factors influencing biofilm geometrical heterogeneity were identified: (a) the ratio between biomass growth rate and internal substrate transfer rate,  $G$  number, (b) external mass transfer limitations as a result of different liquid flow rates, (c) initial substratum surface coverage.
3. Model predictions show that in a biofilm growth regime limited by the rate of substrate transport (internal, as well as external), structures with a high degree of surface irregularity develop. Biofilms grow in these conditions as “finger-like” or filamentous structures with high-surface roughness, high surface area, high porosity, and low degree of compactness. As the nutrient availability

increases, there is a gradual shift towards compact and smooth biofilms.

4. The effects of convection and of flow-driving mechanism on emerging biofilm structures are less important. This is due to the fact that variations in external mass transfer resistance have less effect on biofilm development. The determining factor still seemed to be the internal resistance to substrate transport. This is in agreement with results for various  $G$  ratios, very similar to those obtained in Picioreanu et al. (1988b), when only substrate diffusion was considered through the boundary layer. Probably at low flow velocity a one-dimensional model is sufficient to explain the biofilm geometrical heterogeneity. Although modeling flow seems to be less important for describing substrate transport to biofilm, it will be essential for quantifying biofilm detachment rate.
5. A smaller fraction of the substratum surface colonized led to a rougher biofilm. Surface irregularity and vertical channels deep in the biofilm are, in this case, caused by the inability of the colonies to spread over the whole surface.
6. The substrate flux to the biofilm was greatly influenced by both internal and external mass transfer rates, but not affected by the inoculation density.

All the simulations reported here were performed on the Cray T3E of the Center for High Performance Applied Computing in Technical University Delft. The authors acknowledge Hermann Eberl for many critical and conceptual suggestions.

## References

- Beefink HH, van der Heijden RTJM, Heijnen JJ. 1990. Maintenance requirements: Energy supply from simultaneous endogenous respiration and substrate consumption. *FEMS Microb Ecol* 73:203–209.
- Bishop P, Rittmann BE. 1996. Modeling heterogeneity in biofilms: Report of the discussion session. *Water Sci Tech* 32(8):263–265.
- Characklis WG, Trulear MG, Bryers JD, Zelver N. 1982. Dynamics of biofilm processes: Methods. *Water Res* 16:1207–1216.
- Chen S, Dawson SP, Doolen GD, Janecky DR, Lawniczak A. 1995. Lattice methods and their applications to reacting systems. *Computers Chem Engng* 19(6/7):617–646.
- Chen Y, Ohashi H, Akiyama M. 1997. Simulation of laminar flow over a backward-facing step using the lattice BGK method. *JSME Intl J Series B* 40(1):25–32.
- de Beer D, Stoodley P, Roe F, Lewandowski Z. 1994. Effects of biofilm structures on oxygen distribution and mass transport. *Biotechnol Bioeng* 43:1131–1138.
- de Beer D, Stoodley P. 1995. Relation between the structure of an aerobic biofilm and transport phenomena. *Water Sci Technol* 32(8):11–18.
- Eberl H, Picioreanu C, van Loosdrecht MCM. 1999. Modelling geometrical heterogeneity in biofilms. In: *Proceedings of The 13th International Conference of High Performance Computing Systems & Applications*, June 1999, Kingston, Canada.
- Gjaltema A, Arts PAM, van Loosdrecht MCM, Kuennen JG, Heijnen JJ. 1994. Heterogeneity of biofilms in rotating annular reactors: Occurrence, structure and consequences. *Biotechnol Bioeng* 44:194–204.
- Gjaltema A, van der Marel N, van Loosdrecht MCM, Heijnen JJ. 1997. Adhesion and biofilm development on suspended carriers in airlift reactors: Hydrodynamic conditions versus surface characteristics. *Biotechnol Bioeng* 55:880–889.
- Hermanowicz SW. 1998. A model of two-dimensional biofilm morphology. *Water Sci Technol* 37:219–222.
- Hermanowicz SW. 1999. Two-dimensional simulations of biofilm development: Effects of external environmental conditions. *Water Sci Technol* 39(7):107–114.
- Kwok WK, Picioreanu C, Ong SL, van Loosdrecht MCM, Ng WJ, Heijnen JJ. 1998. Influence of biomass production and detachment forces on biofilm structures in a biofilm airlift suspension reactor. *Biotechnol Bioeng* 58(4):400–407.
- Kugaprasatham S, Nagaoka H, Ohgaki S. 1992. Effect of turbulence on nitrifying biofilms at non-limiting substrate conditions. *Water Res* 26(12):1629–1638.
- Picioreanu C. 1996. Modelling biofilms with cellular automata. Final report to European Environmental Research Organisation, April 1996, Wageningen, The Netherlands.
- Picioreanu C, van Loosdrecht MCM, Heijnen JJ. 1998a. A new combined differential-discrete cellular automaton approach for biofilm modeling: Application for growth in gel beads. *Biotechnol Bioeng* 57(6):718–731.
- Picioreanu C, van Loosdrecht MCM, Heijnen JJ. 1998b. Mathematical modeling of biofilm structure with a hybrid differential-discrete cellular automaton approach. *Biotechnol Bioeng* 58(1):101–116.
- Picioreanu C, van Loosdrecht MCM, Heijnen JJ. 1999. Discrete-differential modelling of biofilm structure. *Water Sci Technol* 39(7):115–122.
- Picioreanu C. 1999. Multidimensional modeling of biofilm structure. PhD Thesis, Delft University of Technology, The Netherlands.
- Picioreanu C, van Loosdrecht MCM, Heijnen JJ. 2000. A theoretical study on the effect of surface roughness on mass transport and transformation in biofilms. *Biotechnol Bioeng* 68:354–369.
- Picologlou BF, Zelver N, Characklis WG. 1980. Biofilm growth and hydraulic performance. *J Hyd Div ASCE* 106:733–746.
- Ponce Dawson S, Chen S, Doolen GD. 1993. Lattice Boltzmann computations for reaction-diffusion equations. *J Chem Phys* 98(2):1514–1523.
- Rittmann BE, Manem JA. 1992. Development and experimental evaluation of a steady-state, multispecies biofilm model. *Biotechnol Bioeng* 39:914–922.
- Rittmann BE, Pettis M, Reeves HW, Stahl DA. 1999. How biofilm clusters affect substrate flux and ecological selection. *Water Sci Technol* 39(7):99–105.
- van Loosdrecht MCM, Lyklema J, Norde W, Schraa G, Zehnder AJB. 1987. Electrophoretic mobility and hydrophobicity as a measure to predict the initial steps of bacterial adhesion. *Appl Environ Microbiol* 53:1898–1901.
- van Loosdrecht MCM, Eikelboom D, Gjaltema A, Mulder A, Tjihuis L, Heijnen JJ. 1995. Biofilm structures. *Water Sci Technol* 32(8):235–243.
- van Loosdrecht MCM, Picioreanu C, Heijnen JJ. 1997. A more unifying hypothesis for the structure of microbial biofilms. *FEMS Microb Ecol* 24:181–183.
- Verran J, Lees G, Shakespeare AP. 1991. The effect of surface roughness on the adhesion of *Candida albicans* to acrylic. *Biofouling* 3:183–192.
- Wanner O, Gujer W. 1986. Multispecies biofilm model. *Biotechnol Bioeng* 28:314–328.
- Wimpenny JWT, Colasanti R. 1997. A unifying hypothesis for the structure of microbial biofilms based on cellular automaton models. *FEMS Microb Ecol* 22:1–16.